PCCP

ROYAL SOCIETY OF CHEMISTRY

PAPER

View Article Online
View Journal | View Issue

Cite this: *Phys. Chem. Chem. Phys.*, 2015, **17**, 27769

The electronic structures of group-V–group-IV hetero-bilayer structures: a first-principles study†

Yanli Wang*[a] and Yi Ding*[b]

Received 13th August 2015,
Accepted 25th September 2015

DOI: 10.1039/c5cp04815j

www.rsc.org/pccp

Recent findings of group-V nanosheets provide new building units for van der Waals hetero-nanostructures. Based on first-principles calculation, we investigate the structural and electronic properties of bilayer hetero-sheets composed of group-V (arsenene/antimonene) and group-IV (graphene/silicene) layers. These hetero-sheets exhibit typical van der Waals features with small binding energies and soft interlayer elastic constants. In the hetero-sheets, the Dirac characteristics of the group-IV layer and the semiconducting feature of the group-V one are well preserved, which causes a Schottky contact at the metal–semiconductor interface. The Schottky barriers are always p-type in the Si-based hetero-sheets, whereas in the C-based ones, the interfacial feature is sensitive to the interlayer distance. A tensile strain would induce a p-type-to-n-type Schottky barrier transition for the As–C hetero-sheet, while a compressive strain can cause a Schottky-to-ohmic contact transition in the Sb–C one. Moreover, due to the inhomogeneous charge redistribution, a sizeable band gap is opened at the Dirac point of the Sb–Si hetero-sheet, which could be linearly modulated by perpendicular strains around the equilibrium site. The versatile electronic structures and tunable interfacial properties enable the group-V–group-IV hetero-bilayer structures to have many potential applications in nano-devices and nano-electronics.

1 Introduction

Since the discovery of phosphorene, two-dimensional (2D) group-V nanosheets have received substantial scientific attention from physicists, chemists, and materials scientists.[1–6] By similar approaches as for graphene, few-layered P nanosheets have been fabricated from black phosphorus by mechanical and liquid exfoliation.[7–10] This black-P sheet is a puckered hexagonal lattice, in which P zigzag lines are alternated up and down in the z direction.[4,5] The structural anisotropy brings some unusual properties to the black-P sheet, such as anisotropic mechanical characteristics with a negative Poisson's ratio,[11–15] orientation-dependent carrier mobilities and thermal transport properties.[16–21] Besides the black-P sheets, theoretical studies also predict that there are several possible buckled conformations co-existing for phosphorene.[22–25] Among them, the blue-P sheet, a chair-buckled honeycomb akin to silicene, is an energetically near-degenerate allotrope of the black-P one.[26–31] Very recently, this chair-like buckled structure has been identified as the ground state for arsenene and antimonene (As and Sb) nanosheets.[32–40] For these As and Sb nanosheets, the corresponding parent bulk materials, *i.e.* the layered grey arsenic and antimony analogues, exist in reality.[41] Experimentally, ultra-thin Sb films, which are composed of multi-layered Sb sheets, have already been prepared.[42] Thus, it is expected that monolayer and few-layered arsenene and antimonene nanosheets could be synthesized as other 2D nanomaterials.[43–45] Akin to phosphorene, theoretical calculations show that these As and Sb nanosheets are also semiconductors with tunable band gaps.[33,34,36,37]

As the new member of 2D nanomaterial, semiconducting group-V nanosheets provide new building units for van der Waals hetero-nanostructures.[46,47] In experiments, phosphorene–MoS_2, phosphorene–TiO_2, phosphorene–BN and phosphorene–graphene hetero-bilayer structures have already been synthesized.[48–50] It shows that the P sheet can form a type-II heterojunction with the MoS_2 sheet, which will be a highly efficient nanomaterial for solar energy.[51,52] For the phosphorene–graphene hetero-sheet, it possesses an intrinsic Schottky contact at the P–C interface, and the Schottky barrier can be modulated by strains and electric fields.[53–56] Motivated by this progress, it is natural to explore hetero-systems composed of arsenene/antimonene and graphene/silicene sheets. Could they form stable van der Waals hetero-bilayer structures?

[a] *Department of Physics, Center for Optoelectronics Materials and Devices, Zhejiang Sci-Tech University, Xiasha College Park, Hangzhou, Zhejiang 310018, People's Republic of China. E-mail: wangyanli-04@tsinghua.org.cn*
[b] *Department of Physics, Hangzhou Normal University, Hangzhou, Zhejiang 310036, People's Republic of China. E-mail: dingyi2001@tsinghua.org.cn*

† Electronic supplementary information (ESI) available: (Fig. S1) The atomic structures and band structures of As(3,1)–C(3,3) and Sb(5,0)–Si(4,2) hetero-sheets, (Fig. S2) The partial charge densities of the valence band and conduction band states at the Dirac point of the Sb–Si hetero-sheet, (Fig. S3) the height distributions of atoms at the interface of As/Sb–C/Si hetero-sheets, (Fig. S4) the minimum and maximum values of the interlayer distances in the As/Sb–C/Si hetero-sheets, and (Table S1) the relative energies for the top, hollow, and bridge site conformations of As/Sb–C/Si hetero-sheets. See DOI: 10.1039/c5cp04815j

Published on 25 September 2015. Downloaded by Pennsylvania State University on 10/05/2016 19:36:16.

Published on 25 September 2015. Downloaded by Pennsylvania State University on 10/05/2016 19:36:16.

Do they possess unique electronic properties? How can we tailor their properties? To address these issues, we perform a comprehensive first-principles investigation on the structures and properties of As–C, Sb–C, As–Si, and Sb–Si hetero-sheets.

2 Methods

The first-principles calculations are performed using the VASP code with the Perdew–Burke–Ernzerhof (PBE) projector augmented wave pseudopotentials.[57,58] Plane-wave basis sets with a cutoff energy of 500 eV are used, and the Grimme-D3 correction (DFT + D3) method is adopted for the dispersion correction in the hetero-bilayer structures.[59,60] To avoid the spurious interaction between replicas, a vacuum layer of about 15 Å is adopted in the calculations. For pristine C, Si, As, and Sb sheets, a 15 × 15 × 1 k-mesh is used to fully relax the lattice constants. The obtained results are shown in Fig. 1, which shows the lattice constants a are 2.47, 3.85, 3.57 and 4.06 Å for C, Si, As, and Sb sheets, and the buckling heights are 0, 0.47, 1.40, and 1.66 Å, respectively. These DFT + D3 results agree well with previous data.[4,33,34]

Due to the various lattice constants, two layers in the hetero-sheets will have different orientations to form a proper super-cell to match each other. Here, following the symmetry of the lattice, the periodical lattices of the As (Sb) layers are set as $\mathbf{a} = m\mathbf{a}_1 + n\mathbf{a}_2$, $\mathbf{a}' = -n\mathbf{a}_1 + (m+n)\mathbf{a}_2$ ($|\mathbf{a}_1| = |\mathbf{a}_2| = a_0$). For the C (Si) layers, they are $\mathbf{b} = p\mathbf{b}_1 + q\mathbf{b}_2$, $\mathbf{b}' = -q\mathbf{b}_1 + (p+q)\mathbf{b}_2$ ($|\mathbf{b}_1| = |\mathbf{b}_2| = b_0$). The lattice mismatch between two different layers is

$$\Delta = \frac{\left|a_0\sqrt{m^2+n^2+mn} - b_0\sqrt{p^2+q^2+pq}\right|}{\left(a_0\sqrt{m^2+n^2+mn} + b_0\sqrt{p^2+q^2+pq}\right)/2}$$

and the rotation angle θ between them is[61]

$$\theta = \arccos\left(\frac{mp+nq+(mq+np)/2}{\sqrt{m^2+n^2+mn}\times\sqrt{p^2+q^2+pq}}\right)$$

The parameter space of (m,n)–(p,q) is scanned to seek out commensurable supercells that satisfy $\Delta < 1\%$. Owing to the computational constraints, supercells with the minimum total atom number $\left(N = 2\times\left(\sqrt{m^2+n^2+mn}+\sqrt{p^2+q^2+pq}\right)\right)$ are used in the calculations. For all the hetero-bilayer systems, the dipole correction is applied in the calculations. It is found that the total energy change is about 0.1 eV per supercell without the dipole correction. During structural relaxation, all the atomic coordinates of the supercells are fully optimized until the maximum residual force is less than 0.01 eV Å^{-1}.

3 Results and discussion

The group-V–group-IV hetero-sheet is a bilayer structure, which is composed of an As/Sb layer and a C/Si layer. The optimized results of (m,n)–(p,q) for As/Sb–C/Si hetero-sheets are listed in Table 1, which are (3,0)–(3,2) for As–C, (5,1)–(3,3) for As–Si, (2,1)–(3,2) for Sb–C, and (3,2)–(4,1) for the Sb–Si ones. The corresponding lattice mismatch Δ, rotation angle θ, and total atom number N are also provided in Table 1. The non-zero value of θ suggests the moiré pattern will appear in these bilayer systems. For each hetero-sheet, three possible conformations have been considered, in which the upper As/Sb atom at the origin is located at the top, hollow, or bridge site of the lower C/Si layer. The relative energies of the top, hollow, and bridge site conformations are listed in Table S1 of the ESI.† It shows that in the As/Sb–C hetero-sheets, the total energy of the hollow site conformation is about 1–6 meV lower than the other conformations, and the energy differences are increased to 5–25 meV in the Sb–Si hetero-sheet. While for the As–Si one, the bridge site conformation has a lower energy than the hollow and top ones by about 3 and 14 meV, respectively. Thus, the As–Si hetero-sheet prefers the bridge site conformation, while the other three hetero-sheets favour the hollow site one as depicted in Fig. 2(a)–(d). These stable conformations are used as the representatives of As/Sb–C/Si hetero-sheets hereafter.

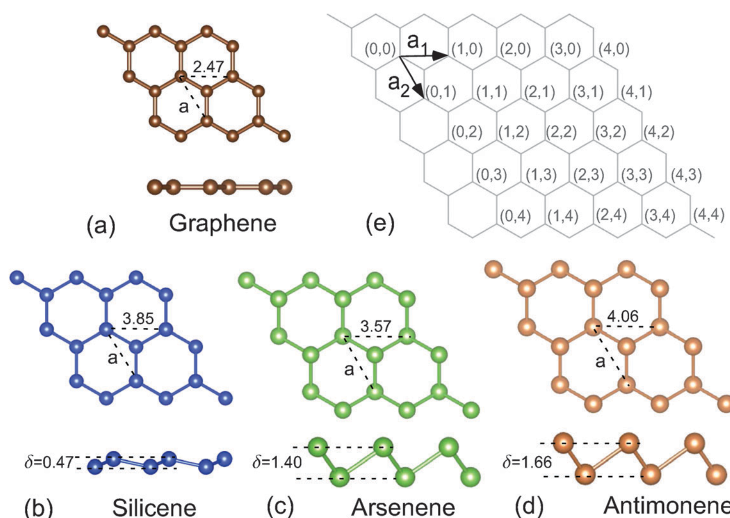

Fig. 1 (a–d) The structures of graphene (C), silicene (Si), arsenene (As) and antimonene (Sb) nanosheets. (e) The representation (m,n) (or (p,q)) stands for the periodical lattice in the honeycomb sheet.

This journal is © the Owner Societies 2015

Published on 25 September 2015. Downloaded by Pennsylvania State University on 10/05/2016 19:36:16.

Table 1 The structural parameters of the group-V–group-IV hetero-sheets. (*m*,*n*) and (*p*,*q*) stand for the periodical lattice of As/Sb and C/Si layers, respectively. *a* is the lattice length of supercell for As/Sb–C/Si hetero-sheets. Δ and θ are the lattice mismatch and rotation angle between As/Sb and C/Si layers. *N*, *h*, and *E* are the total atom number, interlayer distance, and binding energy of the hetero-sheets. Since the in-plane coordinates are not identical in the two layers, the interlayer distance *h* is calculated as the difference between the average heights of atoms at the interface in the upper and bottom layers of hetero-sheets. The corresponding height distribution of interfacial atoms in the hetero-sheets and the maximum/minimum values of interlayer distance are depicted in Fig. S3 and S4 of the ESI

	(*m*,*n*)	(*p*,*q*)	*a* (Å)	*N*	Δ (%)	θ (°)	*h* (Å)	*E* (meV Å^{-2})
As–C	(3,0)	(3,2)	10.72	56	0.53	23.4	3.60	−15.6
As–Si	(5,1)	(3,3)	19.89	116	0.64	21.1	3.01	−25.3
Sb–C	(2,1)	(3,2)	10.75	52	0.23	4.3	3.51	−15.1
Sb–Si	(3,2)	(4,1)	17.71	80	0.31	12.5	2.98	−26.1

To determine the stability of the hetero-sheets, the binding energies are calculated using $E_b = E_{hetero} - E_{As/Sb} - E_{C/Si}$, where E_{hetero} is the total energy of the As/Sb–C/Si hetero-sheet, $E_{As/Sb}$ and $E_{C/Si}$ are the energies of the isolated As/Sb and C/Si monolayer sheets, respectively. Fig. 1(e) and (f) plot the variation of binding energies *versus* the interlayer distances (h) for the As/Sb–C/Si hetero-sheets. It shows that the minimum binding energies of As–C and Sb–C are −15.6 and −15.1 meV Å^{-2} at h = 3.60 and 3.51 Å, and they are −25.3 and −26.1 meV Å^{-2} for As–Si and Sb–Si at h = 3.01 and 2.98 Å, respectively. All these values of E_b are comparable to that of the bilayer graphene (−18.6 meV Å^{-2} by our DFT + D3 calculation), which suggests that the As/Sb–C/Si hetero-sheets are typical van der Waals systems. Besides that, since the As/Sb and C/Si sheets share the same C_{3v} lattice symmetry, the interactions between two layers are stronger than the phosphorene-based hetero-systems. Thus, the binding energies of the As/Sb–C/Si hetero-sheets are a bit smaller than the P–C (−9.4 meV Å^{-2} [56] and −10.4 to −7.6 meV Å^{-2} [54]) and P–MoS$_2$ (−12.7 meV Å^{-2} [52]) ones. In experiments, P–C and P–MoS$_2$ sheets have already been produced.[48,50] Hence, the favoured E_b of the As/Sb–C/Si hetero-bilayer structures indicates the robust stability of the As/Sb-based van der Waals systems, which will be feasible for the production in experiments.

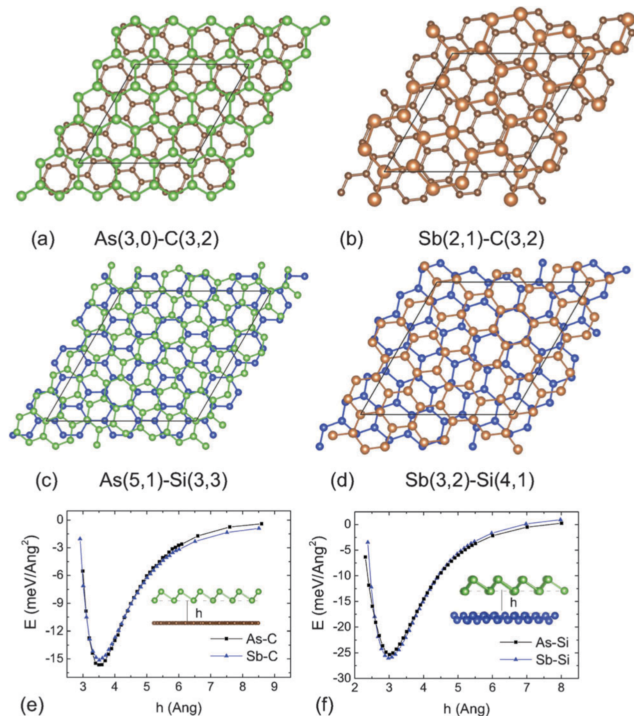

Fig. 2 The structures of (a) As–C, (b) Sb–C, (c) As–Si, and (d) Sb–Si hetero-sheets. The binding energies as a function of interlayer distances for the (e) As/Sb–C and (f) As/Sb–Si ones.

As shown in Fig. 1(e) and (f), the E–h curves of As/Sb–C/Si hetero-sheets exhibit specific intermolecular interaction features, which can be fitted to an empirical potential within a Buckingham (Exp-6) form:[62]

$$E(h) = \frac{\varepsilon}{1-6/\alpha}\left[\left(\frac{6}{\alpha}\right)\exp\left[\alpha\left(1-\frac{h}{h'}\right)\right] - \left(\frac{h'}{h}\right)^6\right].$$

Here, the fitting parameters ε and h' correspond to the depth and site of the energy well, and α is a dimensionless quantity representing the steepness of the repulsive part. For the As–C hetero-sheet, a nonlinear fitting process gives ε = 15.5 meV Å^{-2}, h' = 3.52 Å, and α = 3.40, and for the As–Si one, they are ε = 25.4 meV Å^{-2}, h' = 2.95 Å, and α = 2.67. The quantities of the Sb–C and Sb–Si hetero-sheets are similar to those of the As-based ones as shown in Table 2. It should be noted that besides the intermolecular features, there are no direct chemical bonds or charge transfer between the layers. Thus, the interlayer interaction in the hetero-sheets will not be the covalent or ionic bonding types. The fitted ε (or E_b from the first-principles) values are in the range of physical adsorption for layered materials[63] and the $h'(h)$ values are also close to the interlayer distance in typical van der Waals systems.[64] These results suggest that the weak interaction in the As/Sb–C/Si hetero-sheets is the van der Waals type, which results in small interlayer elastic constants C_{33}. Based on the empirical analytic expression, this interlayer elastic constant (C_{33}) along the normal direction can be evaluated as $C_{33} = \frac{h}{S}\frac{\partial^2 E}{\partial h^2}\Big|_{h=h'}$.[54,64] For the As–C and Sb–C sheets, the C_{33} values are calculated to be 19.9 and 17.2 GPa, and for the As–Si and Sb–Si ones, the C_{33} increases to 28.7 and 30.8 GPa, respectively. Compared with the phosphorene–graphene hetero-sheets (C_{33} = 28 GPa[54]) and bilayer graphene (C_{33} = 38 GPa[64]), the As/Sb–Si ones show similar rigidity, while the As/Sb–C ones are much softer. Therefore, just like other van der Waals systems, the low values of C_{33} mean that the interlayer distance of the As/Sb–C/Si hetero-sheets can be easily tailored by perpendicular strains.

Table 2 The fitted Buckingham parameters for the binding energies and interlayer elastic constant of group-V–group-IV hetero-sheets

	ε (meV Å^{-2})	h' (Å)	α	C_{33} (GPa)
As–C	15.5	3.52	3.40	19.9
As–Si	25.4	2.95	2.67	28.7
Sb–C	14.9	3.52	3.13	17.2
Sb–Si	26.2	2.94	2.75	30.8

Published on 25 September 2015. Downloaded by Pennsylvania State University on 10/05/2016 19:36:16.

It should be noted that the discrepancies in h, E_b and C_{33} between As/Sb–Si and As/Sb–C systems stem from the intrinsic difference between silicene and graphene. Graphene has a flat plane, while silicene has a buckled structure, which is favourable for reducing the Pauli repulsion from the As/Sb layer. More importantly, the Si atom has a larger polarizability than the C atom, which causes a stronger van der Waals interaction between the As/Sb sheet and silicene. Due to the stronger binding strength, the As/Sb–Si hetero-sheets have smaller interlayer distances h, lower binding energies E_b and larger interlayer elastic constants C_{33} than the As/Sb–C systems.

Fig. 3 displays the band structures of the As–C and Sb–C hetero-sheets, showing the contributions from the C layer are separated from the As/Sb ones. The Dirac cone is still kept in the C layer and no band gap is opened at the Dirac point. The Fermi level is across the Dirac point, indicating charge neutrality for the C layer in the As–C and Sb–C hetero-sheets. Since there is no charge transfer between the layers, the semiconducting characteristics are also preserved in the As and Sb layers. The corresponding band gaps are 1.52 and 1.16 eV for the As and Sb ones, respectively, very close to the values (1.51 and 1.13 eV) of the isolated arsenene and antimonene sheets. Similar to the phosphorene–graphene hetero-bilayer structure,[53,56] the semi-metallic C layer and the semiconducting As/Sb one form a Schottky contact at the interface. According to the Schottky–Mott rule, the corresponding Schottky barrier height (SBH) is determined from the energy positions of band edges in the semiconductor and the Fermi level in the metal.[65] Here the p-/n-type SBH values are calculated from the energy differences between the Dirac point of the C layer and the valence band maximum (VBM)/conduction band minimum (CBM) of the As/Sb layer. In the Sb–C sheet, as shown in Fig. 2(d), the Dirac point is close to the top valence band of the Sb layer. The Δ_{VB} is 0.05 eV, much smaller than the Δ_{CB} of 1.12 eV. Thus, it is a typical p-type Schottky contact in the Sb–C interface. In the As–C one, the Δ_{VB} and Δ_{CB} are 0.71 and 0.81 eV, which also exhibits a p-type feature for the Schottky contact. It would be noted that previous studies have shown that when a noticeable interaction exists in the interface, it will perturb the electronic structure of the semiconducting part and pin the Fermi level, which leads to the failure of the Schottky–Mott rule.[66,67] While in this work, all the As/Sb–C/Si hetero-sheets are van der Waals bilayer systems, in which the bands of the semiconducting layers are well preserved. Thus, akin to the case of graphene–phosphorene,[53,56] the Schottky–Mott rule will also be valid in the As/Sb–C/Si hetero-sheets.

In these As/Sb–C hetero-sheets, the SBH values can be further modulated by the perpendicular strains, which even alter the contact features. As shown in Fig. 4(a) and (b), when the distance between the As/Sb and C layers is larger than 5 Å, the Δ_{VB}/Δ_{CB} converges to 1.04/0.48 and 0.45/0.70 eV for the As–C and Sb–C hetero-sheets, respectively. This suggests that the Schottky contact of the Sb–C system is still p-type, but the As–C one turns out to be n-type. Such transformation is attributed to the different work functions (WF) of arsenene, antimonene and graphene. The band alignment between isolated As, Sb, and C sheets are depicted in Fig. 4(c), which shows that their WFs are 4.52, 4.12, and 4.26 eV, respectively. Upon combining with the gap of 1.52 eV, the Dirac point of graphene will be closer to the CBM than the VBM of arsenene. Thus, from the view of the isolated case, the Schottky barrier would involuntarily be n-type when the interlayer distance of the As–C sheet is large enough. As shown in Fig. 4(a), starting from the equilibrium site, the Δ_{VB} (Δ_{CB}) is increased (decreased) when h is increased. The conversion point of SBH, where $\Delta_{VB} = \Delta_{CB}$, is about $\Delta h = 0.1$ Å. Utilizing the fitted Buckingham formula, we estimate that it corresponds to a tensile pressure of 0.48 GPa to induce the p-type-to-n-type

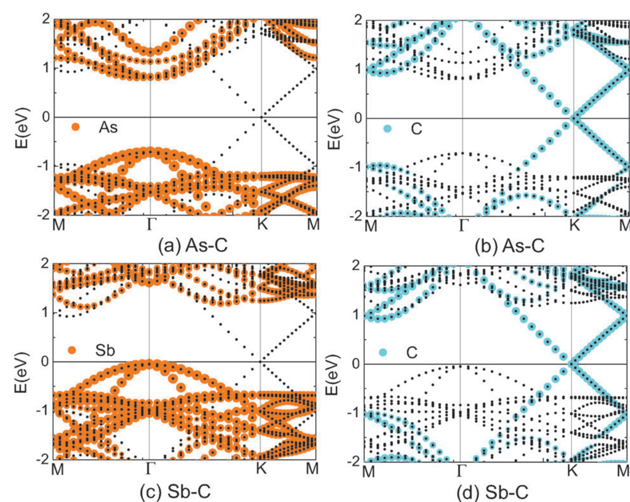

Fig. 3 The band structures of ((a) and (b)) As–C and ((c) and (d)) Sb–C hetero-sheets. The bands projected to As/Sb and C orbitals are highlighted by orange and cyan circles, and the size corresponds to the weight of each species in the bands.

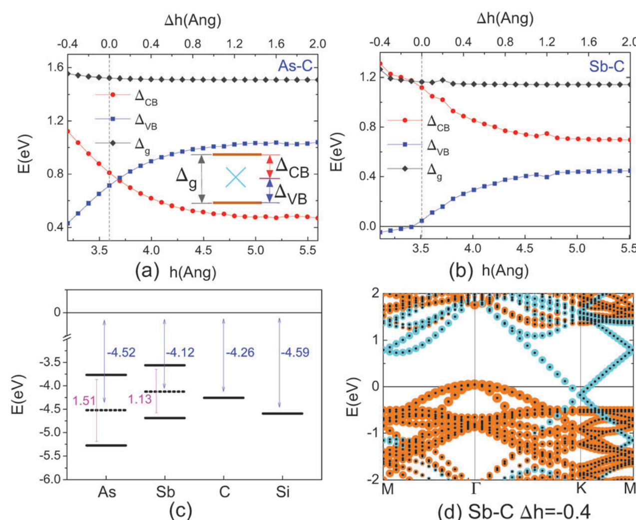

Fig. 4 The variations of Schottky barriers for (a) As–C and (b) Sb–C hetero-sheets. (c) The band alignment of band edges for isolated As, Sb, C, and Si nanosheets, where the zero point is adopted to the vacuum level. (d) The band structures of the Sb–C hetero-sheet under a compression strain of $\Delta h = -0.4$ Å, where the bands projected to Sb and C orbitals are also highlighted by orange and cyan circles, and the size corresponds to the weight of each species in the bands.

View Article Online

Published on 25 September 2015. Downloaded by Pennsylvania State University on 10/05/2016 19:36:16.

Schottky barrier transition in the As–C hetero-sheet. For the Sb–C one, the variation of h does not change its SBH feature, which is always p-type as shown in Fig. 3(b). However, it would be noted that when $\Delta h \leq -0.1$ Å, the Δ_{VB} value becomes negative. This means that the Dirac point of the C layer is below the VBM of the Sb layer. As shown in Fig. 4(d), the Fermi level crosses the valence bands of the Sb layer and the conduction bands of the C layer. Such metallicity transforms the Schottky contact to an ohmic contact at the Sb–C interface. Based on the fitted Buckingham formula, we estimate that the required compressive pressure is about 0.58 GPa for the Schottky-to-ohmic transition in the Sb–C hetero-sheet.

The electronic structures of the As/Sb–Si hetero-sheets are depicted in Fig. 5. Akin to the As/Sb–C ones, their band structures are also a superposition of the Dirac-like properties of the Si layer and the semiconducting character of the As/Sb layer. Due to the special supercells of $p - q = 3k$ (k is an integer), the Dirac point of the Si layer is folded to the Γ point. In the As–Si hetero-sheet, a tiny band gap of 0.008 eV is opened at the Dirac point, and in the Sb–Si one the gap is increased to 0.09 eV. Despite the small band gaps, the As/Sb–Si hetero-sheets still possess a Schottky contact at their interface. The $\Delta_{\mathrm{VB}}/\Delta_{\mathrm{CB}}$ values are 0.66/0.96 and 0.30/0.88 eV for the As–Si and Sb–Si hetero-sheets, respectively, indicating the p-type SBHs for both systems. Such p-type feature is robust against perpendicular strains as shown in Fig. 5(c) and (d).

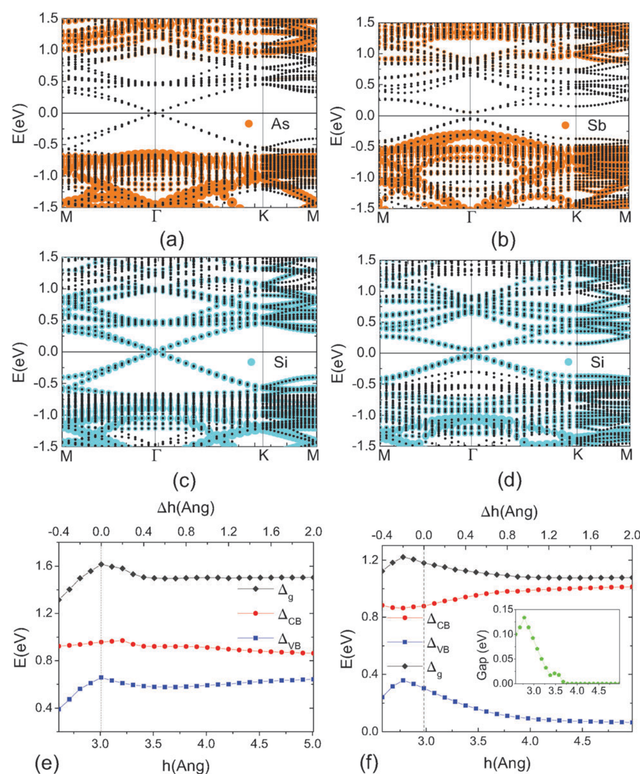

Fig. 5 The band structures of ((a) and (c)) As–Si and ((b) and (d)) Sb–Si hetero-sheets. The bands projected to As/Sb and Si orbitals are highlighted by orange and cyan circles, and the size corresponds to the weight of each species in the bands. The variations of Schottky barriers for (e) As–Si and (f) Sb–Si hetero-sheets. The inset of (f) depicts the variations of the opened band gap at the Dirac point *versus* the interlayer distance.

The Δ_{VB} is always smaller than the Δ_{CB} in the As/Sb–Si hetero-sheets. When h is large, their Δ_{VB} converges to 0.64 and 0.06 eV for the As–Si and Sb–Si ones, which is consistent with the band alignment of the isolated As, Sb, and Si cases shown in Fig. 4(c). The p-type SBHs in hetero-sheets are related to the isolated cases as $\Delta_{\mathrm{VB}} = E_{\mathrm{C}} - E_{\mathrm{VBM}} - \Delta V$, where E_{C} and E_{VBM} are the absolute energies of the Dirac point in graphene and the valence band maximum (VBM) in the As/Sb layer, and ΔV is the potential step formed at the interface.[67] Based on the data in Fig. 4(a) and (b), ΔV can be estimated to be 0.33/0.44 eV in the As/Sb–C hetero-sheets, which are analogous in the two systems. Thus, the SBHs are strongly dependent on the E_{VBM} of the semiconducting layer. Since the E_{VBM} of the Sb layer is closer to the E_{C} of graphene, the Sb–C hetero-sheet has a much smaller Δ_{VB} than the As–C one, which leads to a stronger p-type feature. We have also performed additional calculations on larger supercells such as As(3,1)–C(3,3) and Sb(5,0)–Si(4,2) hetero-sheets, which also satisfy the lattice mismatch constraint of less than 1%. The corresponding band structures are plotted in Fig. S1 of the ESI,† which are analogous to the ones of As(3,0)–C(3,2) and Sb(3,2)–Si(4,1) in Fig. 3 and 5. It indicates that the obtained electronic and interfacial properties of the hetero-sheets are insensitive to the used (m,n)–(p,q) values of supercells.

Compared with the phosphorene–graphene (P–C) hybrid system,[53,56] the p-type-to-n-type Schottky barrier transition is only present in the As–C hetero-sheet, while other systems possess a robust p-type feature against strains. The electronic properties of As/Sb–C/Si hetero-sheets are more versatile than the P–C ones. The C layer is still gapless on the As/Sb sheets, while the Si layer opens a small band gap due to the substrate effect. Particularly, a Schottky-to-ohmic contact transition occurs in the Sb–C hetero-sheet, which has not been reported in the P–C system. These distinct electronic and interfacial properties enable the As/Sb–C/Si hetero-sheets to have many potential applications in nano-electronics and nano-devices.

Finally, it would be noted that among the As/Sb–C/Si hetero-sheets, only the Sb–Si one opens a sizeable band gap at the Dirac point. In order to gain more insight into this phenomenon, the charge density difference of the hetero-sheets is calculated, which is defined as $\Delta\rho = \rho_{\mathrm{hetero}} - \rho_{\mathrm{As/Sb}} - \rho_{\mathrm{C/Si}}$. Here, ρ_{hetero} is the total charge density of the As/Sb–C/Si hetero-sheet, $\rho_{\mathrm{As/Sb}}$ and $\rho_{\mathrm{C/Si}}$ are the charge densities of the isolated As/Sb and C/Si layers with the same positions in the hetero-sheet. Fig. 6(a)–(d) display the plane-integrated $\Delta\rho$ perpendicular to the hetero-sheets. It can be seen that there are some charge redistributions in the interval between the two layers. For the As/Sb–C systems, such redistributions are small as shown in Fig. 6(a) and (b), whose peaks are only up to $\sim$0.1 e Å^{-1}, too small to affect the Dirac-like band structure of graphene. Whereas in the As/Sb–Si hetero-sheets, the redistribution is remarkable, for which the maximum of the peaks is about 1 e Å^{-1}, Fig. 6(c) and (d). When we integrate the positive region in the interlayer space, the charge accumulations are obtained as 0.54 and 0.60 e for the As–Si and Sb–Si hetero-sheets, which are much larger than the values of 0.06 and 0.08 e in the As–C and As–Si ones. Obviously, the charge redistributions are more pronounced in the As/Sb–Si sheets,

Published on 25 September 2015. Downloaded by Pennsylvania State University on 10/05/2016 19:36:16.

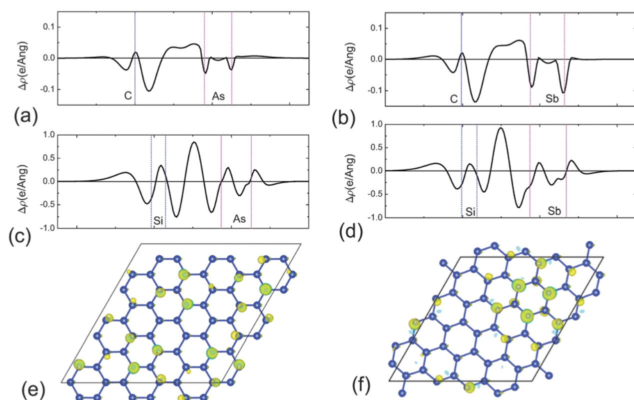

Fig. 6 The plane-integrated change density differences for the (a) As–C, (b) Sb–C, (c) As–Si, (d) Sb–Si hetero-sheets. The cross view on the charge density difference of (e) As–Si and (f) Sb–Si systems.

which stem from the stronger interlayer coupling and the smaller distance between the As/Sb and silicene layers. As a result, the Dirac-like properties of the Si layer are significantly modified. For the silicene one, owing to its bi-particle feature, the band gap of the Dirac point will depend on the on-site difference between the two sublattices.[68,69] In Fig. 6(c) and (d), a cross view on the charge density difference of the As/Sb–Si systems is provided. For the As–Si hetero-sheet, the accumulated charges are located on the top of some Si atoms, which are evenly distributed in the supercell. While in the Sb–Si one, the charges prefer to be accumulated on one sublattice locally in the top right corner. The corresponding partial charge densities of the valence band and conduction band states at the Dirac point are depicted in Fig. S2 of the ESI.† It can be seen that the two valence band states are composed of the Si p_z orbitals at the outside of hetero-sheet, while the two conduction band states are made up of the Si p_z orbitals in the inside region, pointing towards the Sb layer. As a result, the sublattice symmetry of silicene is broken by the Sb substrate, and the Coulomb repulsion between the layers pushes the conduction band states to higher energies than the valence band states, which causes the gap opening in the Sb–Si hetero-sheet. When the interlayer distance of Sb–Si becomes larger, the effects of charge redistribution will be weaker. Thus, the band gap is reduced under tensile perpendicular strains on the Sb–Si hetero-sheet, for which the zero-band-gap feature appears when $h \geq 3.8$ Å. On the other hand, a compressive interlayer strain will enhance the charge redistribution effect, which increases the band gap. Around the equilibrium site, a linear gap–strain relationship can be seen in the range of $\Delta h = -0.2$–0.4 Å. The slope, *i.e.* deformation potential, is about 0.2 eV Å^{-1} for the Sb–Si hetero-sheet. Combining with the fitted Buckingham formula, it suggests that the gap of the Sb–Si hetero-sheet can be controllably varied from 145% to 55% when the pressure is in a range from the compression of 3.13 GPa to the tension of 1.44 GPa. This tunable band gap of the Sb–Si hetero-bilayer structure enables it to be a promising candidate as a nano-mechanical sensor.

Experimentally, the compressive pressure can be easily generated on 2D materials by a common diamond anvil cell method. For instance, a high pressure of up to 50–60 GPa has been applied to few-layered graphene, MoS_2, and $MoSe_2$ sheets in the experiments.[70–72] Here, for the As/Sb–C/Si hetero-sheets, the required pressure is of the magnitude of 0.5–3.1 GPa, which is affordable in experiments. On the other hand, controllable tensile pressure on the nanosheets is still a challenge currently. Since the effect of tensile pressure is to expand the interlayer distance, this can be achieved by using the intercalation technique. In the experiments, through controlling the relative humidity, the inserted water molecules could gradually increase the interlayer distance by about 1 Å in the bilayer graphene oxide.[73] Thus, upon utilizing these advanced experimental methods, the effective pressure would be applied to the As/Sb–C/Si systems, which changes the interlayer distances and modulates their electronic and interfacial properties.

4 Conclusion

In summary, we have investigated the electronic structures of group V–group IV hetero-bilayer structures. Due to the same lattice symmetry of As, Sb, C, and Si nanosheets, commensurable supercells are found for the hetero-sheets, which reduce the mismatch of two layers and enhance the stabilities of the hetero-bilayer structures. The binding energies of As/Sb–C and As/Sb–Si hetero-sheets are about −15 and −25 meV Å^{-2}, stronger than the phosphorene-based ones. The intrinsic electronic properties of As/Sb and C/Si sheets are well preserved in these hetero-bilayer structures, which form a p-type Schottky contact in these semiconductor–metal interfaces. The Schottky barrier can be tuned by perpendicular strains, which can induce a p-type-to-n-type Schottky barrier transition for the As–C hetero-sheet and a Schottky-to-ohmic contact transition in the Sb–C one. Moreover, due to the inhomogeneous charge redistribution in the interval, a sizeable band gap is opened at the Dirac point of the Sb–Si hetero-sheet, which can be tailored by perpendicular strains with a linear varying trend around the equilibrium site. Our study demonstrates that the As/Sb nanosheets would form the stable hetero-bilayer structures with the graphene and silicene ones, which have versatile electronic structures and tunable interfacial properties for nano-devices and nano-electronics applications.

Acknowledgements

The authors acknowledge the support from the National Natural Science Foundation of China under Grant No. 11474081 and the Zhejiang Provincial Natural Science Foundation of China under Grant No. LY15A040008. Some of the calculations were performed at the Shanghai Supercomputer Center of China.

References

1 L. Li, Y. Yu, G. J. Ye, Q. Ge, X. Ou, H. Wu, D. Feng, X. H. Chen and Y. Zhang, *Nat. Nanotechnol.*, 2014, **9**, 372–377.

2 H. Liu, A. T. Neal, Z. Zhu, Z. Luo, X. Xu, D. Tomanek and P. D. Ye, *ACS Nano*, 2014, **8**, 4033–4041.

This journal is © the Owner Societies 2015

Published on 25 September 2015. Downloaded by Pennsylvania State University on 10/05/2016 19:36:16.

3 F. Xia, H. Wang and Y. Jia, *Nat. Commun.*, 2014, **5**, 4458.
4 S. Balendhran, S. Walia, H. Nili, S. Sriram and M. Bhaskaran, *Small*, 2015, **11**, 640–652.
5 H. Liu, Y. Du, Y. Deng and P. D. Ye, *Chem. Soc. Rev.*, 2015, **44**, 2732–2743.
6 X. Ling, H. Wang, S. Huang, F. Xia and M. S. Dresselhaus, *Proc. Natl. Acad. Sci. U. S. A.*, 2015, **112**, 4523–4530.
7 J. O. Island, G. A. Steele, H. S. J. van der Zant and A. Castellanos-Gomez, *2D Mater.*, 2015, **2**, 011002.
8 J. R. Brent, N. Savjani, E. A. Lewis, S. J. Haigh, D. J. Lewis and P. O'Brien, *Chem. Commun.*, 2014, **50**, 13338–13341.
9 P. Yasaei, B. Kumar, T. Foroozan, C. Wang, M. Asadi, D. Tuschel, J. E. Indacochea, R. F. Klie and A. Salehi-Khojin, *Adv. Mater.*, 2015, **27**, 1887–1892.
10 L. Kou, C. Chen and S. C. Smith, *J. Phys. Chem. Lett.*, 2015, 2794–2805.
11 Q. Wei and X. Peng, *Appl. Phys. Lett.*, 2014, **104**, 251915.
12 J.-W. Jiang and H. S. Park, *Nat. Commun.*, 2014, **5**, 5727.
13 Y. Ding, Y. Wang, L. Shi, Z. Xu and J. Ni, *Phys. Status Solidi RRL*, 2014, **8**, 939–942.
14 L. Kou, Y. Ma, S. C. Smith and C. Chen, *J. Phys. Chem. Lett.*, 2015, **6**, 1509–1513.
15 L. Wang, A. Kutana, X. Zou and B. I. Yakobson, *Nanoscale*, 2015, **7**, 9746–9751.
16 R. Fei and L. Yang, *Nano Lett.*, 2014, **14**, 2884–2889.
17 Z.-Y. Ong, G. Zhang and Y. W. Zhang, *J. Appl. Phys.*, 2014, **116**, 214505.
18 Y. Xu, J. Dai and X. C. Zeng, *J. Phys. Chem. Lett.*, 2015, **6**, 1996–2002.
19 A. Jain and A. J. H. McGaughey, *Sci. Rep.*, 2015, **5**, 8501.
20 T.-H. Liu and C.-C. Chang, *Nanoscale*, 2015, **7**, 10648–10654.
21 G. Qin, Q.-B. Yan, Z. Qin, S.-Y. Yue, M. Hu and G. Su, *Phys. Chem. Chem. Phys.*, 2015, **17**, 4854–4858.
22 J. Guan, Z. Zhu and D. Tománek, *Phys. Rev. Lett.*, 2014, **113**, 046804.
23 J. Guan, Z. Zhu and D. Tománek, *ACS Nano*, 2014, **8**, 12763–12768.
24 M. Wu, H. Fu, L. Zhou, K. Yao and X. C. Zeng, *Nano Lett.*, 2015, **15**, 3557–3562.
25 G. Yu, L. Jiang and Y. Zheng, *J. Phys.: Condens. Matter*, 2015, **27**, 255006.
26 Z. Zhu and D. Tománek, *Phys. Rev. Lett.*, 2014, **112**, 176802.
27 J. Xie, M. S. Si, D. Z. Yang, Z. Y. Zhang and D. S. Xue, *J. Appl. Phys.*, 2014, **116**, 073704.
28 Y. Ding and Y. Wang, *J. Phys. Chem. C*, 2015, **119**, 10610–10622.
29 B. Ghosh, S. Nahas, S. Bhowmick and A. Agarwal, *Phys. Rev. B: Condens. Matter Mater. Phys.*, 2015, **91**, 115433.
30 J. Xiao, M. Long, X. Zhang, J. Ouyang, H. Xu and Y. Gao, *Sci. Rep.*, 2015, **5**, 9961.
31 L. Hu, J. Zhao and J. Yang, *Nanoscale*, 2015, **7**, 8962–8967.
32 S. Zhang, Z. Yan, Y. Li, Z. Chen and H. Zeng, *Angew. Chem., Int. Ed.*, 2015, **54**, 3112.
33 C. Kamal and M. Ezawa, *Phys. Rev. B: Condens. Matter Mater. Phys.*, 2015, **91**, 085423.
34 Z. Zhu, J. Guan and D. Tománek, *Phys. Rev. B: Condens. Matter Mater. Phys.*, 2015, **91**, 161404.
35 G. Wang, R. Pandey and S. P. Karna, *ACS Appl. Mater. Interfaces*, 2015, **7**, 11490–11496.
36 Y. Wang and Y. Ding, *J. Phys.: Condens. Matter*, 2015, **27**, 225304.
37 Z. Zhang, J. Xie, D. Yang, Y. Wang, M. Si and D. Xue, *Appl. Phys. Express*, 2015, **8**, 055201.
38 P. Chun-Ying, Y. Xiao-Tao, J. Hua-Long, Z. Fei-Wu, L. Zhi-Wen, H. Jun-Bao and Z. Da-Wei, *Chin. Phys. B*, 2015, **24**, 036301.
39 Y. Wang and Y. Ding, *Nanoscale Res. Lett.*, 2015, **10**, 254.
40 L. Kou, Y. Ma, X. Tan, T. Frauenheim, A. Du and S. Smith, *J. Phys. Chem. C*, 2015, **119**, 6918–6922.
41 *Chemistry of Arsenic, Antimony and Bismuth*, ed. N. Norman, Springer, Netherlands, 1998.
42 G. Yao, Z. Luo, F. Pan, W. Xu, Y. P. Feng and X.-s. Wang, *Sci. Rep.*, 2013, **3**, 2010.
43 P. Avouris and C. Dimitrakopoulos, *Mater. Today*, 2012, **15**, 86–97.
44 Y. Yamada-Takamura and R. Friedlein, *Sci. Technol. Adv. Mater.*, 2014, **15**, 064404.
45 S. Das, M. Kim, J.-w. Lee and W. Choi, *Crit. Rev. Solid State Mater. Sci.*, 2014, **39**, 231–252.
46 A. K. Geim and I. V. Grigorieva, *Nature*, 2013, **499**, 419–425.
47 D. Tomanek, *J. Phys.: Condens. Matter*, 2015, **27**, 133203.
48 Y. Deng, Z. Luo, N. J. Conrad, H. Liu, Y. Gong, S. Najmaei, P. M. Ajayan, J. Lou, X. Xu and P. D. Ye, *ACS Nano*, 2014, **8**, 8292–8299.
49 H. Uk Lee, S. C. Lee, J. Won, B.-C. Son, S. Choi, Y. Kim, S. Y. Park, H.-S. Kim, Y.-C. Lee and J. Lee, *Sci. Rep.*, 2015, **5**, 8691.
50 A. Avsar, I. J. Vera-Marun, J. Y. Tan, K. Watanabe, T. Taniguchi, A. H. Castro Neto and B. Ozyilmaz, *ACS Nano*, 2015, **9**, 4138–4145.
51 J. Dai and X. C. Zeng, *J. Phys. Chem. Lett.*, 2014, **5**, 1289–1293.
52 L. Huang, N. Huo, Y. Li, H. Chen, J. Yang, Z. Wei, J. Li and S.-S. Li, *J. Phys. Chem. Lett.*, 2015, 2483–2488.
53 J. E. Padilha, A. Fazzio and A. J. R. da Silva, *Phys. Rev. Lett.*, 2015, **114**, 066803.
54 Y. Cai, G. Zhang and Y.-W. Zhang, *J. Phys. Chem. C*, 2015, **119**, 13929–13936.
55 P. Rivero, C. M. Horvath, Z. Zhu, J. Guan, D. Tománek and S. Barraza-Lopez, *Phys. Rev. B: Condens. Matter Mater. Phys.*, 2015, **91**, 115413.
56 W. Hu, T. Wang and J. Yang, *J. Mater. Chem. C*, 2015, **3**, 4756–4761.
57 G. Kresse and J. Furthmuller, *Comput. Mater. Sci.*, 1996, **6**, 15–50.
58 G. Kresse and J. Furthmuller, *Phys. Rev. B: Condens. Matter Mater. Phys.*, 1996, **54**, 11169–11186.
59 S. Grimme, J. Antony, S. Ehrlich and H. Krieg, *J. Chem. Phys.*, 2010, **132**, 154104.
60 S. Grimme, S. Ehrlich and L. Goerigk, *J. Comput. Chem.*, 2011, **32**, 1456–1465.
61 L. Li and M. Zhao, *J. Phys. Chem. C*, 2014, **118**, 19129–19138.
62 E. A. Mason, *J. Chem. Phys.*, 1954, **22**, 169–186.
63 T. Björkman, A. Gulans, A. V. Krasheninnikov and R. M. Nieminen, *Phys. Rev. Lett.*, 2012, **108**, 235502.
64 X. Chen, F. Tian, C. Persson, W. Duan and N.-x. Chen, *Sci. Rep.*, 2013, **3**, 3046.

Published on 25 September 2015. Downloaded by Pennsylvania State University on 10/05/2016 19:36:16.

65 R. T. Tung, *Appl. Phys. Rev.*, 2014, **1**, 011304.
66 C. Gong, L. Colombo, R. M. Wallace and K. Cho, *Nano Lett.*, 2014, **14**, 1714–1720.
67 M. Farmanbar and G. Brocks, *Phys. Rev. B: Condens. Matter Mater. Phys.*, 2015, **91**, 161304.
68 R. Quhe, R. Fei, Q. Liu, J. Zheng, H. Li, C. Xu, Z. Ni, Y. Wang, D. Yu, Z. Gao and J. Lu, *Sci. Rep.*, 2012, **2**, 0852.
69 N. D. Drummond, V. Zólyomi and V. I. Fal'ko, *Phys. Rev. B: Condens. Matter Mater. Phys.*, 2012, **85**, 075423.
70 S. Clark, K.-J. Jeon, J.-Y. Chen and C.-S. Yoo, *Solid State Commun.*, 2013, **154**, 15–18.
71 A. P. Nayak, S. Bhattacharyya, J. Zhu, J. Liu, X. Wu, T. Pandey, C. Jin, A. K. Singh, D. Akinwande and J.-F. Lin, *Nat. Commun.*, 2014, **5**, 3731.
72 Z. Zhao, H. Zhang, H. Yuan, S. Wang, Y. Lin, Q. Zeng, G. Xu, Z. Liu, G. K. Solanki, K. D. Patel, Y. Cui, H. Y. Hwang and W. L. Mao, *Nat. Commun.*, 2015, **6**, 7312.
73 B. Rezania, N. Severin, A. V. Talyzin and J. P. Rabe, *Nano Lett.*, 2014, **14**, 3993–3998.

This journal is © the Owner Societies 2015